Environmental Science and Pollution Research (2023) 30:110161–110174
https://doi.org/10.1007/s11356-023-30086-7

RESEARCH ARTICLE

Manganese oxide–loaded activated carbon for ammonium removal from wastewater: the roles of adsorption and oxidation

Yifei Wang[1] · Xingyi Jiang[1] · Xinshan Song[1] · Xin Cao[1] · Zhongshuo Xu[1] · Yuhui Wang[1] · Jianfeng Li[2] · Nan Wu[3] · Junhong Bai[4]

Received: 23 June 2023 / Accepted: 21 September 2023 / Published online: 2 October 2023

Abstract

The urgent need to address the severe issue of nitrogen pollution has prompted the search for a functional and easy recycling material. In this study, manganese oxides (MnO_x) were loaded on activated carbon (AC), resulting in a composite known as AC-MnO_x, for efficient ammonium removal from aqueous solutions. The results indicated a remarkable 15.6-fold increase in ammonium removal efficiency and a fivefold enhancement in removal capacity for AC-MnO_x (3.20 mg/g) compared to AC. Under specific conditions (initial NH_4^+-N concentration of 15 mg/L, adsorbent dose of 2.5 g, pH of 6.5, and temperature of 35 ℃), the highest achieved ammonium removal efficiency reached 94.6%. Furthermore, the study distinguishes the contributions of catalytic oxidation and adsorption in the removal process. The adsorption process was effectively modeled using pseudo-second-order kinetics and Langmuir isotherm models. Interestingly, the amount of oxidation conversion (N_{tur}) exhibited a linear relationship with the dosage when the initial ammonium concentration was sufficiently high, while the relationship between initial ammonium concentration and the ratio of N_{tur} to adsorption capacity (N_{sur}) followed a negative exponential trend. The removal mechanisms involved electrostatic interaction between ammonium and the negatively charged dehydrogenated hydroxyl groups ($-OH_{sur}$) or cation tunnel in crystal structures of MnO_x, ion exchange adsorption, and the oxidation impact of MnO_x. This research provides valuable insights into the application of immobilized MnO_x media for ammonium removal. Moreover, filling AC-MnO_x into constructed wetlands (CW) proved to be an effective method for reducing ammonium pollution, demonstrating its potential in the field of engineering wastewater treatment.

Keywords Ammonium removal · Manganese oxides · Adsorption · MnO_x catalytic oxidation · Ammonium conversion mechanism

Responsible Editor: Tito Roberto Cadaval Jr

✉ Xinshan Song
newmountain@163.com

[1] State Environmental Protection Engineering Center for Pollution Treatment and Control in Textile Industry, College of Environmental Science and Engineering, Donghua University, Shanghai 201620, China

[2] State Environmental Protection Key Laboratory of Efficient Resource Utilization Techniques of Coal Waste, Institute of Resources and Environmental Engineering, Shanxi Collaborative Innovation Center of High Value-Added Utilization of Coal-Related Wastes, Shanxi University, Taiyuan 030006, China

[3] China Institute of Water Resources and Hydropower Research, Beijing 100038, China

[4] School of Environment, Beijing Normal University, Beijing 100875, China

Introduction

Nitrogen pollution is a pervasive environmental issue confronting the world today, leading to eutrophication, damaging human health, and posing a threat to biodiversity (Cheng et al. 2019; Peng et al. 2018). Ammonium in surface water or groundwater is the primary contributor to nitrogen pollution (Girotto et al. 2020). Thus, finding effective and viable strategies for the rapid removal of ammonium has long been an important subject for researchers, including biological and physicochemical methods (Vocciante et al. 2018).

Although microbial nitrification played an important role in the ammonium removal (Cheng et al. 2019; Liu et al. 2019), microorganism activities were affected by variable environmental conditions significantly, such as temperature, the pH value, and dissolved oxygen (DO) (Ducey et al. 2010; Rajeshwari et al. 2000). The growth and the activity

of nitrifying bacteria were inhibited under conditions of low temperature (< 15 °C) (Andersson et al. 2001), low DO concentration (Tatari et al. 2016), and acidic or alkaline (Li et al. 2013). Compared with the biological method, the physicochemical method was considered advantageous for removing ammonium from water conveniently and stably (Chiban et al. 2011a; Cheng et al. 2019; Qiang et al. 2020). It mainly focused on oxidation and adsorption by some kind of composite materials (Chiban et al. 2011b; Li et al. 2015b; Kankanamge et al. 2018). However, they have the drawbacks of a complicated preparation process, low sustainability, and secondary pollution (Cai et al. 2015). Thus, it is an urgent need for an efficient composite material to overcome these disadvantages.

Metal oxide loading was an emerging chemical modification method for adsorption and/or oxidation, which contribute to enhancing the adsorption capacity (Li et al. 2017), broadening the pH adaptability (Tan et al. 2023), and even incorporating catalyst-like properties, such as active manganese oxide (MnO_x) loading media (Cheng et al. 2018). Due to the strong oxidization property of Mn(III) ($E_{Mn(III)/Mn(II)}{}^0 = +1.50$ V) and Mn(IV) ($E_{Mn(IV)/Mn(II)}{}^0 = +1.23$ V), manganese oxides were widely used to remove toxic compounds (Xie et al. 2018; Joshi et al. 2017; Forrez et al. 2009) and can participate in the biochemical cycle of many elements, such as nitrogen, sulfur, and iron (Lin and Taillefert 2014; Wang et al. 2018; Tebo et al. 2005). As a result of physical and chemical properties, open-framework (layered) structure, a large amount of vacancy sites, and negative surface charges in a wide range of pH, MnO_x is regarded as a highly reactive agent for the adsorption and redox transformation of cations (Gadde and Laitinen 1974; Zhao et al. 2018; Wang et al. 2018). Multiple studies have confirmed the catalytic activity of manganese-loaded composite materials in environmental remediation (Lee et al. 2013; Chen et al. 2023). The catalytic activity of MnO_x films in biological filters can improve the efficiency of pollutant removal while reducing the consumption of DO (Yang et al. 2019; Huang et al. 2014). Organic matter was preferentially oxidized by MnO_x, rather than oxygen (Xie et al. 2018).

Previous work inferred that MnO_x could remove ammonium through adsorption and oxidation under low oxygen concentrations in the constructed wetlands (CW) (Li et al. 2021; Wang et al. 2022). However, there was rarely a study on the abiotic effect of MnO_x for ammonium removal. Currently, synthetic manganese oxides have been applied as an adsorbent in wastewater treatment (Cheng et al. 2017b; Zhang et al. 2020). Unfortunately, the application of this powdery material was holden back because of reservation difficulty and secondary pollution. Moreover, the chemical catalytic oxidation of ammonium by MnO_x was ignored in the research, compromising the credibility of the results. Thus, the immobilized MnO_x on the granular medium was considered to be a promising method for wastewater treatment.

As a common adsorption material in wastewater treatment, activated carbon (AC) with substantially lower cost has been widely applied due to its high porosity and large specific surface area (Li et al. 2020; Lyu et al. 2020; Xue et al. 2023). Besides, adjustable surface properties endowed AC with a more powerful performance in removing contaminants after being modified through physical and/or chemical treatment (Zhao et al. 2015; Kolodziej et al. 2014; Xue et al. 2023). It is not clear, whether loading MnO_x displays an improved ammonium removal performance of AC for ammonium. Furthermore, the application of composite materials in full-scale filters or CW systems has become a crucial criterion for assessing their effectiveness (Wang et al. 2023). Recently, Fe–Mn co-oxide composites have been successfully applied to enhance nutrient removal in CWs or filters, achieving 90% and 73.81% ammonium removal, respectively (Guo et al. 2017; Zhang et al. 2019). Therefore, it is worth investigating whether MnO_x-loaded AC can be organically integrated into biological nitrogen removal scenarios, thereby alleviating the constraints of climate conditions on ammonium removal performance.

In this study, MnO_x was loaded on AC to form AC-MnO_x. The substance characterization, surface charge, and functional group structure for different adsorbents were measured by X-ray photoelectron spectroscope (XPS), scanning electron microscope (SEM), Brunauer–Emmett–Teller (BET), ZETA potential, and Fourier transform infrared spectroscopy (FT-IR). Prepared AC-MnO_x was adopted for investigating ammonium elimination in an aqueous solution through batch experiments. Subsequently, the influence of environmental impact factors on the removal of ammonium would be explored. Furthermore, the contributions of catalytic oxidation and adsorption were distinguished. Several kinds of kinetics and isothermal models were used to identify the adsorption characteristic. The removal mechanism was deeply deduced by discussing the effects of environmental factors on the ratio of catalytic oxidation to adsorption. Finally, the feasibility of using AC-MnO_x in CW fillers to enhance the nitrogen removal from wastewater was investigated.

Materials and methods

Preparation of AC-MnO_x

Coconut shell AC with a diameter of 2 to 3 mm was purchased in Henan, China. AC-MnO_x was prepared through the redox precipitation in consideration of the facile preparation procedure and cost-effective feature. Firstly, 10 g of

AC was added into 50 mL of 0.5 mol/L $KMnO_4$ solution under agitation at 400 ± 1 rpm for 1440 min and the purple color of the solution faded so that MnO_x was formed on AC quickly at 298 K. The added $KMnO_4$ concentration was selected based on the results of preliminary experiments with different composition, and from an economic perspective (Fig. S1). Then, the solid was separated and washed with distilled water and absolute ethanol until the pH of the filter liquor was close to neutral, which ensured that $KMnO_4$ on the surface of the AC-MnO_x was reduced. The obtained solid granulars were dried for 360 min at 378 K and designated as AC-MnO_x.

Characterization of AC-MnO_x

The morphology of AC-MnO_x was analyzed by SEM with energy dispersive X-ray spectroscopy (SEM–EDS, S-4800, Japan Electronics Co., Ltd), the transmission electron microscopy (TEM), and the crystal structure was investigated by XRD (Dmax2550VBPC, Rigaku, Japan). The functional groups of AC-MnO_x were identified by an FT-IR spectrophotometer. (Nicolet 6700, Thermal Fisher, USA). The chemical states of MnO_x were investigated by XPS (Escalab 250 Xi, Thermal Fisher, USA). The surface potentials of materials were detected by a ZETA analyzer (Brook Haven 90 PALS, USA). The specific surface area of the adsorbent was determined with the BET-specific surface analysis device (Autosorb-iQ, Quantachrome, USA). The concentrations of ammonia, nitrate and nitrite were determined by a UV–vis spectrophotometer (UV-2000, Unico, China) in triplicate according to "Standard Analysis Methods for the Examination of Water and Wastewater."

Ammonium removal experiment

Effects of external conditions on the ammonium removal

To test the ammonium removal performance of AC-MnO_x, 100 mL of 5 mg/L NH_4Cl solution was added into a 150-mL conical flask to carry out the static removal experiment. The stability of the ammonium removal efficiency of the two materials was investigated under different treatment conditions (dosage (0.1, 0.5, 1.0, 1.5, 2.0, and 2.5 g), temperature (288, 298, and 308 K), and pH (3.5, 5.0, 6.5, 8.0, and 9.5)). The initial pH was carefully adjusted with 0.1 mol/L HCl or 0.1 mol/L NaOH to avoid repeated adjustments and minimize any potential influence on the solution properties (Nguyen et al. 2021; Nouaa et al. 2023). The static experiment was performed under agitation at 130 ± 1 rpm for 24 h. To ensure the sufficient reaction, the reaction time was extended to 24 h.

Adsorption experiments

To explore the adsorption equilibrium time, the adsorption kinetics and isotherm were studied, based on the equilibrium time. The materials were added into 100 mL of NH_4Cl solutions with different concentrations (5, 10, 15, and 25 mg/L). At 288, 298, and 308 K, the experiment was completed at different concentrations. Then, the solution was filtered through a filter with a pore diameter of 0.45 μm for the subsequent detection. Then, the adsorption process was tested under various conditions to explore its kinetics and isotherms. The solid samples were dried at 30 ℃ for further characterization. The ammonium removal involves two mechanisms, catalytic oxidation and adsorption (Lin et al.; Yang et al. 2019; Huang et al. 2014). Thus, the adsorption kinetics and isotherm were fitted with the data obtained by subtracting the quantity of catalytic oxidation nitrogen from the total removal quantity in the adsorption experiment. The total removal quantity of ammonium (Q_t, mg/g) at any time t (min, a certain contact time) is calculated as:

$$Q_t = \frac{V \cdot \left(C_0 - C_t\right)}{m}. \tag{1}$$

The equilibrium removal capacity of each sample is calculated as:

$$Q_e = \frac{V \cdot \left(C_0 - C_e\right)}{m} \tag{2}$$

The quantity of nitrate and nitrite generated in catalytic oxidation is regarded as the indicator of ammonium conversion (N_{tur}, mg/L). The relationship between N_{tur} and the quantity of ammonium removed by adsorption (N_{sur}, mg/L) is expressed as:

$$N_{tur} = C_{NO_3^-} + C_{NO_2^-} = C_0 - C_e - N_{sur}. \tag{3}$$

The quantity of ammonium adsorbed onto the adsorbent (q_t, mg/g) at any time t (min, a certain contact time) is calculated as:

$$q_t = \frac{V \cdot \left(C_0 - C_t - N_{tur}\right)}{m} \tag{4}$$

The equilibrium adsorption capacity of each sample is expressed as:

$$q_e = \frac{V \cdot \left(C_0 - C_e - N_{tur}\right)}{m} = \frac{V \cdot N_{sur}}{m} \tag{5}$$

where C_0 (mg/L), C_t (mg/L), $CNO2^-$ (mg/L), CNO_3^- (mg/L), V (L), and m (g) are, respectively, the initial ammonium concentration, the ammonium concentration at t (min), the nitrate concentration, the nitrite concentration, the solution

volume, and the mass of adsorbent; C_e (mg/L) is the equilibrium concentration.

CW application of AC-MnO_x

To demonstrate the adaptability of the prepared adsorption and catalytic oxidation materials in practical application scenarios, AC-MnO_x was used as a functional substrate and filled into CW for comparison with unmodified AC and inert filler quartz sand (QS). The CW was operated in tidal flow and continuous flow modes, to explore the ability of the functional filler filling region to remove ammonium and the overall nitrogen removal effect of CWs with the participation of microorganisms, respectively.

Statistical analysis

All experiments were carried out in replicates and average values were calculated. Analysis of variance (ANOVA) was performed with Microsoft Excel 2010, whereas the *t* test was used to assess the significance of results (p-value < 0.05).

Results and discussion

Characterization of AC-MnO_x

The crystalline phase analysis by XRD indicated that MnO_x was loaded on the surface (Fig. S2). In other words, AC-MnO_x has been successfully synthesized. The surface morphology and elements of AC-MnO_x were respectively analyzed by SEM and EDS (Fig. 1). The AC with a flat surface with uniformly distributed pores transformed into AC-MnO_x with a rough surface composed of a film covered with unevenly distributed aggregates after the in situ redox reaction. According to the result of FT-IR, reactive functional groups on the surface of AC-MnO_x were abundant, suggesting the existence of hydroxyl (Benhiti et al. 2020), C = O (1760–1500 cm^{-1}), C–O (1300–950 cm^{-1}), and Mn–O (550–700 cm^{-1}) (Shen et al. 2020) (Fig. S3). The surface of composite AC-MnO_x comprised approximately 12.3% (atomic, at. %) manganese and 26.3% (at. %) oxygen, closely resembling the MnO_2 elemental ratio (1:2) as observed in the XRD results. Consequently, the loaded proportion of MnO_x on AC was estimated to be around 12.3%.

Removal capacity of AC-MnO_x

Effects of external conditions on the ammonium removal

The ammonium removal performance of AC-MnO_x was higher than AC (Fig. 2a). Under a given concentration, the dosage and temperature were positively correlated with the removal efficiency (Fig. 2a and b), indicating that the ammonium removal reaction was endothermic. However, the removal efficiency tended to be stable if the addition of AC-MnO_x was above 2 g. Therefore, 2 g of AC-MnO_x was determined as the optimal dosage in subsequent experiments. The ammonium removal efficiency of the tested material was improved by 15.6 times after it was combined with MnO_x. The original AC and AC-MnO_x exhibited ammonium removal capacities of 0.51 and 3.20 mg/g, respectively. The modified AC showed a fivefold enhancement in ammonium removal capacity. In comparison to other surface-modified adsorbents, AC-MnO_x demonstrated significant advantages in terms of its particle form and simple modification process, which allowed for flexible application in various environments and high adsorption capacity for effective treatment efficiency (Table 1). The ammonium removal capacity of AC-MnO_x increased with temperature. Figure 2c illustrates the effect of the initial pH on the ammonium removal efficiency of AC-MnO_x at 298 K. The removal efficiency (74.1–85.3%) suggested a wide range of pH adaptability for ammonium removal efficiency of AC-MnO_x. The negative zeta potential indicated negatively charged surface of AC-MnO_x. The enhanced ammonium removal efficiency after MnO_x loaded

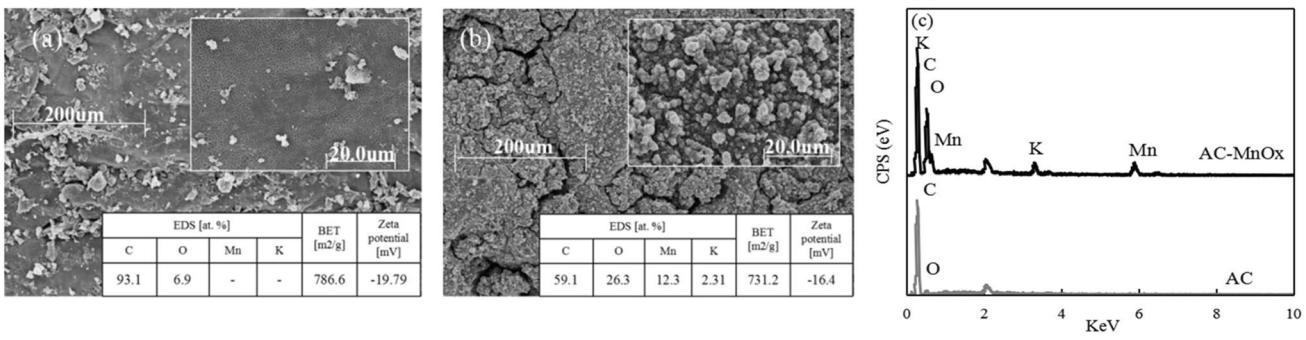

Fig. 1 SEM images and EDS analysis of AC (**a**) and AC-MnO_x (**b**). Energy dispersion spectrum of AC and AC-MnO_x (**c**)

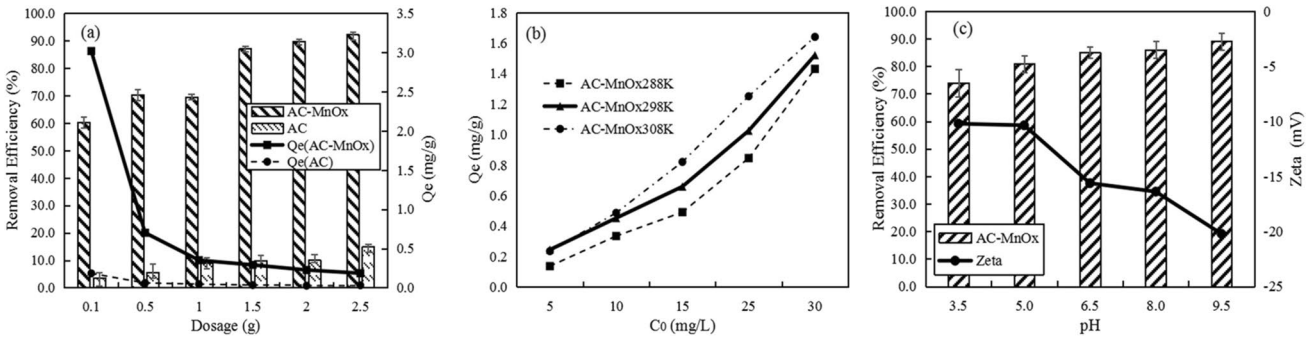

Fig. 2 **a** Removal efficiency and Q_e of AC-MnO_x with different dosages (298 K, C_0 = 5 mg/L); **b** removal capacity of AC-MnO_x at different temperatures (m (AC-MnO_x) = 2 g); **c** removal efficiency of AC-MnO_x and ZETA at different pH (298 K, C_0 = 5 mg/L, m(AC-MnO_x) = 2 g)

Table 1 Adsorption capacities and other parameters for ammonium removal by carbon-based adsorbents with different treatment methods

Adsorbent	Adsorbent form	Capacity (mg/g)	Preparation condition	Reference
Coconut shell-AC	Powder	2.26	Commercially purchased AC	(Bhatnagar et al. 2013)
Coconut shell-AC	Particle	0.51	Commercially purchased AC	This study
AC/HCl-Na	Particle	1.19	AC was modified by acidification pre-treatment by HCl	(Shi et al. 2013)
AC/N-Na	Particle	0.66	AC was modified by Na^+ impregnation after oxidation pre-treatment with HNO_3	(Shi et al. 2013)
MgO-biochar	Particle	22	Porous biochar was impregnated into $MgCl_2$ solution and high-temperature calcination in N_2 atmosphere (500 ℃, 1 h)	(Li et al. 2017)
Nano-Mg-biochar	Powder	23.777	Biochar was impregnated into $MgCl_2$, high-temperature calcination in N_2 atmosphere (450 ℃, 2 h) and then treated by ultrasonic waves	(Tan et al. 2023)
SDS-AC	Particle	1.78	AC was impregnated into sodium dodecyl sulfate (SDS) solution	(Lee et al. 2018)
AC-MnO_x	Particle	3.20	In situ oxidation–reduction (impregnated into $KMnO_4$ solution)	This study

onto AC provided evidence that loading MnO_x improved the removal capacity of AC.

Response surface plots and ammonium removal efficiency

The above experimental results and experimental conditions (Table S2) indicated that pH, initial concentration, dosage, and temperature affected the ammonium removal performance of AC-MnO_x. The removal efficiency of AC-MnO_x was determined through these experiments, and surface response plots were generated for further analysis. The interactions among the dosage (A), pH (B), initial concentration of ammonium (C), and temperature (D) in the ammonium removal by AC-MnO_x were analyzed using central component design (CCD). The three-dimensional response surface plots are shown in Fig. S6. The statistical analysis of variance (ANOVA) was performed on the ammonium removal efficiency data of AC-MnO_x (Table S3). Low p-values (< 0.001) indicated that the four factors had statistically significant effects on the ammonium removal efficiency of AC-MnO_x (Egbosiuba et al. 2020; Schüler et al. 2018). The regression model for the ammonium removal efficiency of AC-MnO_x is described by the following equation:

$$\begin{aligned}\text{Removal efficiency (\%)} = {} & 84.88 + 14.16A + 4.21B - 3.53C + 3.69D \\ & - 1.86AB + 3.88AC - 0.047AD - 0.77BC \\ & - 1.06BD + 1.31CD \\ & - 8A^2 + 0.02B^2 - 0.14C^2 - 1.33D^2 \end{aligned} \quad (7)$$

This model determined the relationship between the four factors and the removal efficiency of AC-MnO_x. As shown in Eq. (7), the higher the coefficient of the influencing factor, the greater its influence on the removal efficiency. An appropriate dosage posed a positive effect on the ammonium removal efficiency of AC-MnO_x. The other three factors had less effect on removal efficiency than dosage, indicating that AC-MnO_x was insensitive to these changes under the given experimental conditions. This stability allowed for efficient ammonium removal under different external changes.

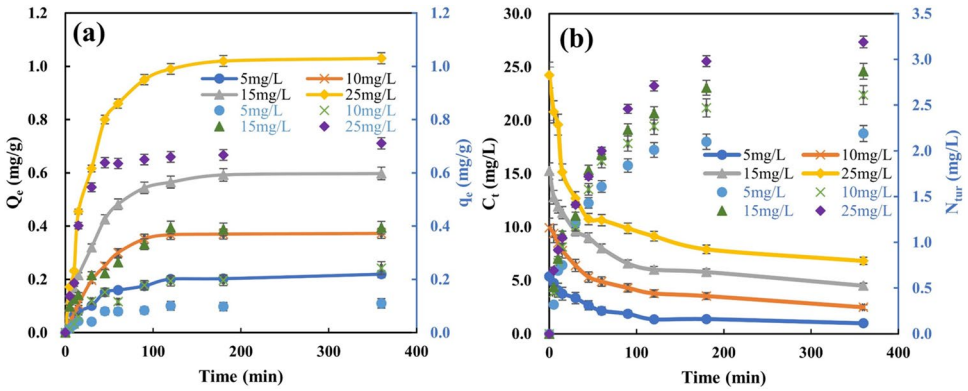

Fig. 3 **a** Effect of contact time on ammonium removal and adsorption on AC-MnO_x; **b** effect of contact time on the ammonium concentration in the solution and the quantity of converted nitrogen at 298 K under different initial concentrations and AC-MnO_x dosage of 2 g. The legend in blue corresponds to the right y-axis

Effect of contact time

To explore the impact of contact time on ammonium removal capacity of AC-MnO_x, Q_e and q_e were evaluated under varying ammonium concentrations. Initially, both rates (Q_e and q_e) showed a rapid increase within the first 60 min, followed by a slower increase over the subsequent 120 min, and eventually reached the equilibrium state after approximately 540 min (Fig. 3a). As the ammonium concentration increased, the maximum q_e of AC-MnO_x also increased from 0.10 to 0.76 mg/g at 298 K. It is worth noting that the catalytic conversion capacity of ammonium was lower than the adsorption capacity. Across different initial concentrations, the catalytic conversion exhibited only a slight variation, ranging from 2.19 to 3.19 mg/L (Fig. 3b). Conversely, the quantity of ammonium removed through adsorption increased significantly from 2.20 to 14.22 mg/L with the rising initial ammonium concentration.

Adsorption experiments

In this section, all adsorption data were determined by subtracting the quantity of catalytic oxidation from the total removal quantity.

Adsorption isotherms

Isotherms describe the equilibrium states between the adsorbate concentrations in the solid phase and in the liquid phase (Fig. S7 and S8), which can be described by the Freundlich and Langmuir equations (Eqs. (S1-S3)) (Karthikeyan et al. 2008). Isotherm parameters for ammonium adsorption onto AC-MnO_x at different temperatures (288 K, 298 K, and 308 K) are provided in Table S4. The regression correlation coefficients (R^2) for the Langmuir model (0.992–0.999) were higher than those for the Freundlich model (0.994–0.991) (Figs. S6-S7). The experimental data demonstrated a good fit with the Langmuir isotherm, indicating that the ammonium adsorption process followed a monolayer adsorption mechanism on the adsorbent surface (Sheela et al. 2012).

Thermodynamic studies

A thermodynamic analysis was performed to examine the adsorption of ammonium on AC-MnO_x at different temperatures (Eqs. (S4-S7)). The distribution coefficient (K_0) of the process increased with temperature, while the Gibbs free energy (ΔG_0) was negatively correlated with temperature (Table S5 and Fig. S9). These results suggest that the spontaneity of the adsorption process was proportional to the temperature (Uğurlu and Karaoğlu 2011). Positive values of ΔH_0 suggested that the adsorption process was endothermic (Cheng et al. 2017a; Egbosiuba et al. 2020). The high ΔH_0 values indicated strong interactions between NH_4^+ ions and the negatively charged sites on the surface of AC-MnO_x (Uğurlu and Karaoğlu 2011). A positive value of ΔS_0 indicated increased disorder and randomness in the adsorption process (Kizito et al. 2015). It was worth noting that ΔH_0 and ΔS_0 were consistently positive, while ΔG_0 was negative at high temperatures and positive at low temperatures (Table S5). This suggested that the adsorption of ammonium by AC-MnO_x was spontaneous at high temperatures, which aligns with the conclusion presented in the "Effects of external conditions on the ammonium removal" section.

Kinetic models

Three kinetic models (pseudo-first-order, pseudo-second-order, and second-order kinetic model) were applied to analyze the adsorption process (q_e), and the fitting curves are displayed in Figs. S10-S12, respectively. The results indicated that the pseudo-second-order model exhibited the highest correlation coefficient among all the models (Table S6), suggesting that the adsorption process was

primarily governed by a chemical reaction (Cai et al. 2020). As the concentration of ammonium in the solution increased, it may stimulate the adsorption onto the deep binding sites of AC-MnO_x. This finding confirmed that the adsorption process was influenced by both the ammonium content in the solution and the availability of active multilayer adsorption sites on AC-MnO_x (Shafiof and Ejhieh 2020).

Ammonium removal mechanism by AC-MnO_x

Changes in AC-MnO_x before and after the reaction

To study the phase changes of Mn species during the oxidation process of ammonium, XPS analysis was carried out on fresh and used AC-MnO_x (Fig. S4). Based on the XPS spectra of the fresh AC-MnO_x (Fig. 4a) and the previously reported peak areas corresponding to different valence states of Mn (Kumar et al. 2016; Li et al. 2015a; Sharma and Zhai 2009), Mn(III) was the dominant valence state in the fresh AC-MnO_x (Liu et al. 2021). Compared with the fresh AC-MnO_x with the used AC-MnO_x, it was observed that the content of Mn(III) decreased while the contents of Mn(II) and Mn(IV) increased in the latter (Fig. 4b). The oxidation state of manganese can be determined by analyzing the satellite separation of Mn3s splitting (ΔEs). Different valence states of Mn exhibit different ΔEs values. The ΔEs (Mn3s) ranges for Mn(IV) and Mn(III) were reported as 4.7–4.8 and 5.3–5.4, respectively (Subramanian et al. 2006; Kim and Shim 2010). The ΔEs for the fresh AC-MnO_x was measured as 5.0 eV (Fig. S5), which falls between the typical ΔEs values of Mn(IV) and Mn(III), indicating the coexistence of Mn(IV) and Mn(III) in the fresh AC-MnO_x. The ΔEs for the used AC-MnO_x was determined as 4.8 eV, which was consistent with the typical ΔEs value of Mn(IV). Based on the relevant data (Table S1), the average oxidation states of Mn in the fresh and used AC-MnO_x were estimated as 3.1 and 3.0, respectively.

In addition, O1s spectra could be used to estimate the oxidation state of manganese. In Fig. 4c and d, the O1s spectra exhibit asymmetry and can be deconvoluted into three peaks at 529.9 eV, 531.0 eV, and 531.8 eV. These peaks were assigned to Mn–O–Mn bonds of tetravalent oxide, Mn–O–H bonds of hydrated trivalent oxide, and H–O–H bonds of residual water, respectively (Sharma and

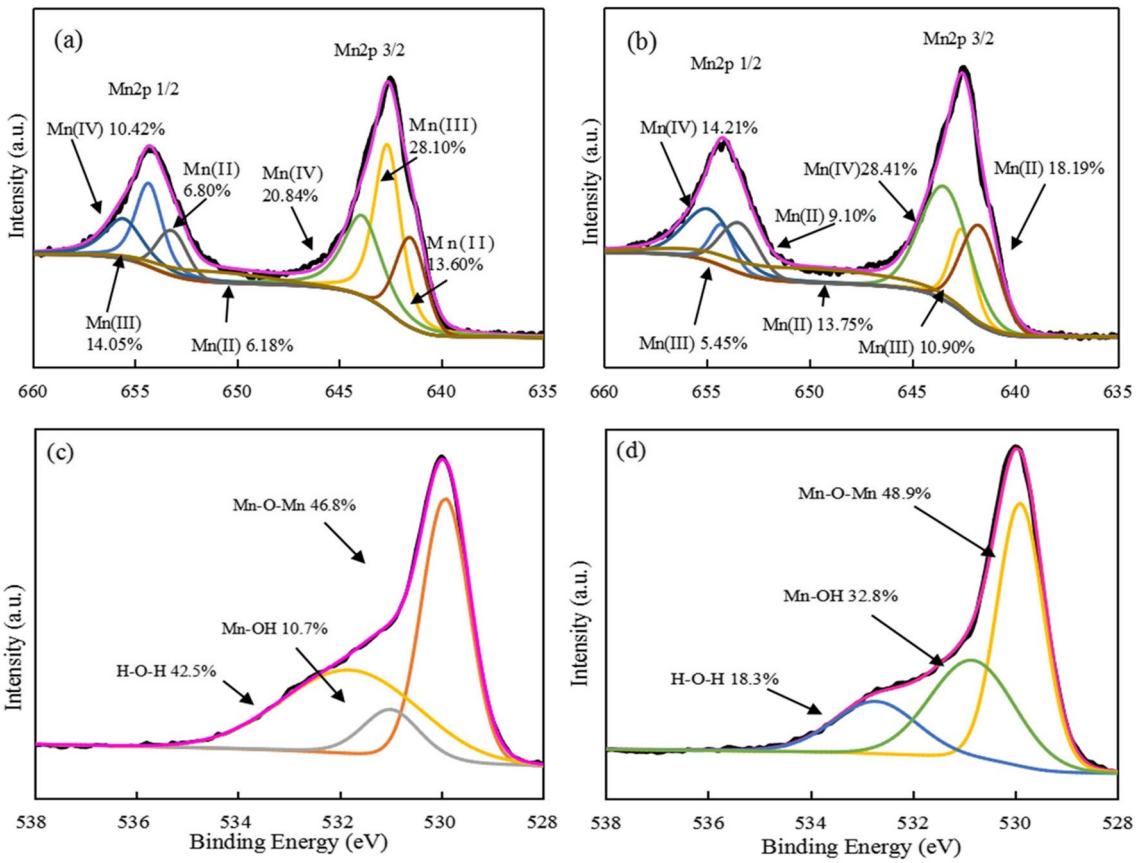

Fig. 4 Mn2p (**a**) and O1s (**c**) XPS spectra of fresh AC-MnO_x. Mn2p (**b**) and O1s (**d**) XPS spectra of used AC-MnO_x

Zhai 2009). The average oxidation state (OS) of Mn can be determined from the intensity of Mn–O–Mn and Mn–O–H peaks (i.e., $S_{Mn-O-Mn}$ and S_{Mn-O-H}) (Toupin et al. 2004):

$$OS = \left(4 \times \left(S_{Mn-O-Mn} - S_{Mn-O-H}\right) + 3 \times S_{Mn-O-H}\right)/S_{Mn-O-Mn} \quad (6)$$

The oxidation state of manganese in the fresh AC-MnO_x (OS = 3.77) was higher than that in the used AC-MnO_x (OS = 3.33). This change in the average valence state of manganese indicated that MnO_x was involved in the oxidation of ammonium.

Catalytic oxidation of ammonium

As previously mentioned, nitrate and nitrite were detected in the solution after the removal of ammonium using AC-MnO_x, while manganese ions were not detected. This implied that AC-MnO_x acted as a catalyst in the oxidation process. The ammonium removal process by AC-MnO_x involved adsorption and catalytic conversion. Thus, the relationship between the ratios of surface adsorption (N_{sur}RE) and catalytic conversion (N_{tur}RE) to total ammonium removal can be expressed as follows:

$$N_{tur}RE\% = \frac{N_{tur}}{N_{sur}+N_{tur}} \times 100\% = 1 - \frac{N_{sur}}{N_{sur}+N_{tur}} \times 100\% = 1 - N_{sur}RE\% \quad (8)$$

To further explore the catalytic conversion rate of AC-MnO_x on ammonium, the relationship between N_{tur}RE and N_{sur}RE was examined under different initial ammonium concentrations (Fig. 5a). As the initial concentration of ammonium increased, the efficiency of ammonium removal decreased. The majority of the total removed ammonium was attributed to adsorption (N_{sur}), while the fraction of ammonium removed through catalytical conversion N_{tur}RE% was significantly lower and reduced with the increasing initial ammonium concentration. This suggested that the catalytic oxidation process occurred at a slower rate compared to adsorption. Initially, a large amount of ammonium was rapidly adsorbed, followed by a decrease in the adsorption rate as adsorption continued.

Figure 5b demonstrates that the catalytic oxidization performance of AC-MnO_x improved gradually with increasing initial ammonium concentration. The value of N_{tur} was positively correlated with the dosage of AC-MnO_x. When the initial ammonium concentration was 25 mg/L, a linear equation with an R^2 of 0.997 was obtained to fit the catalytic conversion of nitrogen with the AC-MnO_x dosage. Under conditions of sufficient ammonium, AC-MnO_x with an equivalent dosage resulted in a similar quantity of catalytic nitrogen oxides (N_{tur}). This indicated that the catalytic oxidation reaction was completed first, accompanied by continuous electrostatic adsorption. However, under the same dosage conditions, the quantity of ammonium adsorbed on the surface (N_{sur}) increased with higher ammonium concentrations. This led to a reduction in the proportion of catalytic oxidation (N_{tur}RE %).

Effects of pH and temperature on N_{tur}/N_{sur}

The pH of the solution had an impact on both the adsorption capacity (*N*sur) and catalytic conversion (N_{tur}) of AC-MnO_x with respect to ammonium (Table 2). Under an initial concentration of 5 mg/L, the N_{tur}/N_{sur} ratio increased as the pH increased (Fig. 6a). In an alkaline environment, ammonium could react with OH– to form NH3·H2O. This reaction reduced the number of ammonium cations available to enter the tunnels within the MnO_x crystals to stabilize the structure (Wang and Li 2003). As a result, when

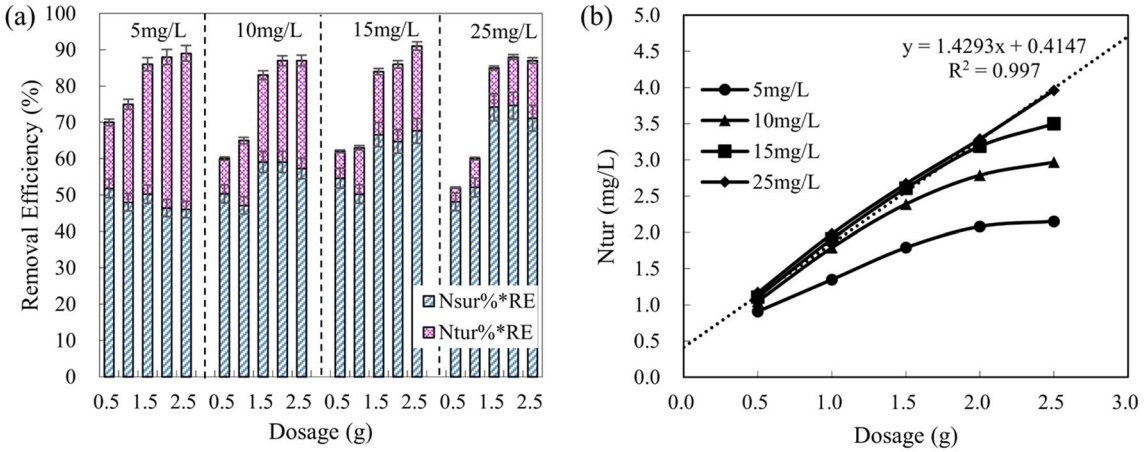

Fig. 5 **a** Proportions of catalytically converted nitrogen (N_{tur}RE%) and adsorbed nitrogen (N_{sur}RE%) in total removal ammonium under the dosages of 0.5, 1, 1.5, 2, and 2.5 g and initial concentrations of 5, 10, 15, and 25 mg/L, and **b** the relationship between the dosage (0.5–2.5 g) and the quantity of catalytically converted nitrogen (N_{tur}) under different initial concentrations (5, 10, 15 and 25 mg/L)

Table 2 Effect of pH0 on ammonium adsorption of AC-MnO_x and N_{tur}RE% under different initial concentrations (298 K)

pH01	Initial concentration of ammonium						ΔpH2	ΔDO3 (mg/L)
	5 mg/L			25 mg/L				
	Qe (mg/g)	*qe* (mg/g)	N_{tur}/N_{sur}	*Qe* (mg/g)	*qe (mg/g)*	N_{tur}/N_{sur}		
3.5	0.19	0.13	0.47	0.99	0.89	0.12	4.21 ± 0.1	−0.41 ± 0.1
5.0	0.20	0.13	0.56	1.05	0.94	0.13	2.82 ± 0.1	−0.37 ± 0.1
6.5	0.21	0.12	0.82	1.10	0.95	0.15	1.05 ± 0.3	−0.48 ± 0.1
8.0	0.22	0.12	0.89	1.11	0.96	0.16	−0.34 ± 0.1	−0.44 ± 0.1
9.5	0.22	0.12	0.93	1.14	0.97	0.18	−1.13 ± 0.1	−0.29 ± 0.1

1pH0 is initial pH

2ΔpH is the change of pH after reaction

3ΔDO is the change of dissolved oxygen; m (AC-MnO_x) = 2 g

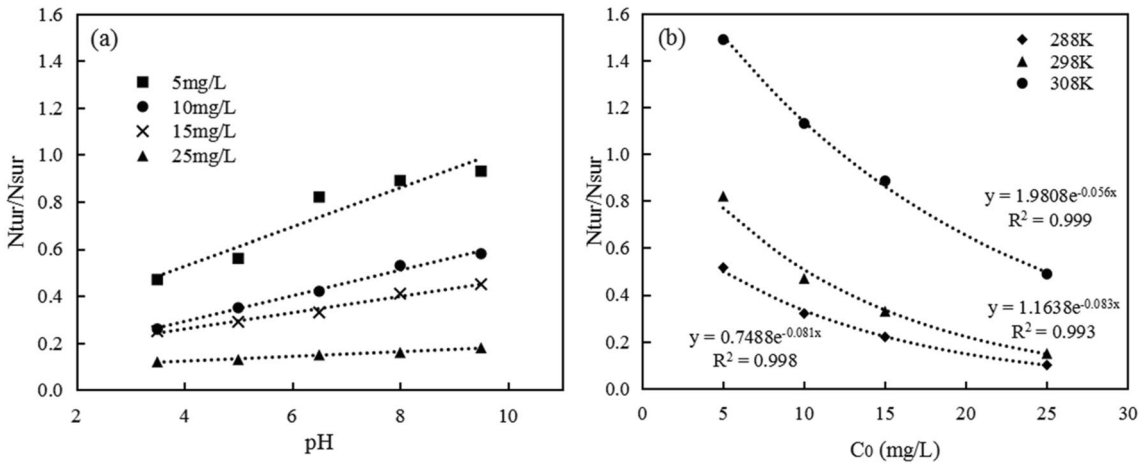

Fig. 6 Effects of **a** pH at 298 K and **b** initial concentration on N_{tur}/N_{sur}. The dashed line represents the linear or nonlinear fitting results of the data points

the pH increased, the proportion of ammonium underwent increase in the catalytic conversion (N_{tur}). Furthermore, the H+ could occupy the binding sites of ammonium and react with MnO_x, resulting in a decrease in N_{tur}RE%. Therefore, in the presence of sufficient OH– ions, a higher N_{tur}RE% could be achieved due to the avoidance of metal ion dissolution caused by high alkalinity.

The initial ammonium concentration showed a negative exponential relationship with N_{tur}/N_{sur} ($R2 = 0.993$–0.998) (Fig. 6b). Furthermore, with an increase in C0, N_{tur}/N_{sur} showed a greater increase at higher temperatures. This suggests that the impact of the initial concentration on catalytic conversion was more significant than on the adsorption process under higher temperatures. Under the same initial concentration, elevated temperatures enhanced the performance of catalytic oxidation, which resulted in an increased N_{tur}/N_{sur} ratio.

Potential adsorption mechanisms

The adsorption mechanism of AC-MnO_x was based on the interactions between the adsorbent and adsorbate NH_4^+, such as physical adsorption, electrostatic attraction, and ion exchange (Hu et al. 2020). AC-MnO_x has a lower surface area but higher NH_4^+-N adsorption capacity, which was contradicted with the expected behavior of physical adsorption. This suggested that physical adsorption was not a major contributor in NH_4^+-N adsorption. Instead, chemical adsorption appeared to be the dominant process, consistent with the observed kinetic results. Although the cation exchange

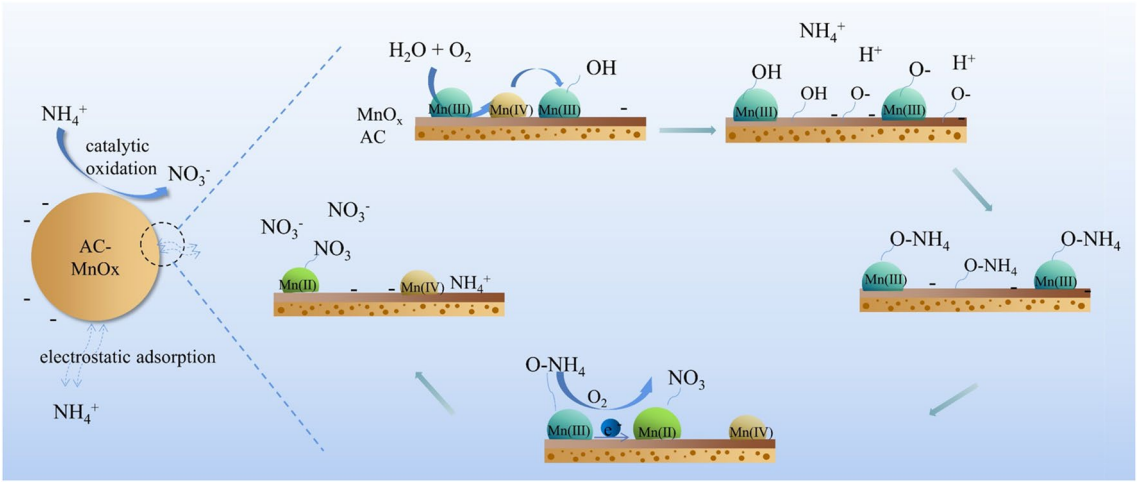

Fig. 7 Mechanism of removal of ammonium by AC-MnO_x

capacity (CEC) of AC-MnO_x was not determined in this work, a previous study found limited NH_4^+-N adsorption capacity through ligand exchange (Nguyen et al. 2021). The loading of MnO_x on AC-MnO_x led to the presence of more surface functional groups, such as hydroxyl, carboxyl, and carbonyl, which contributed to the enhanced NH_4^+ adsorption capacity. Additionally, the high O/C ratio (0.45) of AC-MnO_x resulted in a strongly polar surface (Takaya et al. 2016), promoting electrostatic interactions between NH_4^+ and AC-MnO_x. In general, chemical bonding and electrostatic attraction play predominant roles in the NH_4^+ adsorption process.

Removal mechanisms by catalytic oxidation

Based on the decreasing trend of DO in the solution after the reaction, the catalytic oxidation mechanism can be speculated as follows:

$$2H_2O + O_2 + 4Mn(III) \rightarrow 4Mn(IV) + 4OH^- \quad (9)$$

$$Mn(IV) + H_2O \rightarrow Mn(III) + H^+ + -OHsur \quad (10)$$

The above two reactions (Eqs. (9) and (10)) can be combined as follows:

$$2H_2O + O2 \overset{MnOx}{\rightarrow} 4 - OHsur \quad (11)$$

$$Mn(III) + 2O2 + NH_4^+ \rightarrow Mn(II) + NO_3^- + H2O + 2H^+ \quad (12)$$

The removal mechanism of ammonium by AC-MnO_x could be inferred (Fig. 7). Mn(III) originally present in AC-MnO_x was oxidized to Mn(IV) by DO, resulting in the generation of OH^- (Eq. (9)). Subsequently, Mn(IV) was reduced by H_2O, leading to the regeneration of $–OH_{sur}$ and the release of H^+ ions (Eq. (10)) (Wang et al. 2014; Meng et al. 2020). This reduction/oxidation process involving Mn species occurred. The combination of these reactions can be expressed in Eq. (11). Furthermore, OH^- ions, escaping from the surface groups ($–OH_{sur}$), such as C–OH, –COOH and Mn–OH, caused the surface of AC-MnO_x to become negatively charged (Guo

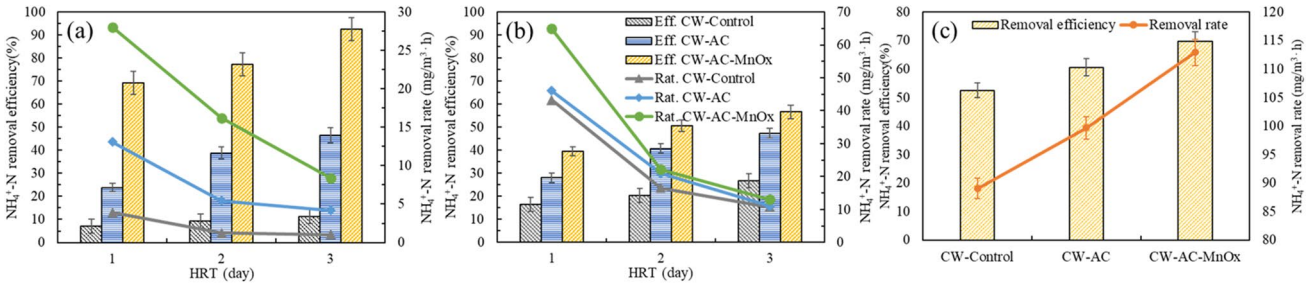

Fig. 8 NH_4^+-N removal performance of AC-MnO_x filling CW: the average NH_4^+-N removal rate and efficiency for the functional layer of intermittent flow CWs in the **a** phase I and **b** phase II (HRT 1 ~ 3 days, five cycles for a total of 15 days), and **c** for the continuous flow CW in the phase III (15 mg/L influent NH_4^+-N, HRT 1 day, five cycles). Removal efficiency and rate were calculated as the average value over five cycles

et al. 2017; Zhao et al. 2018). As a result, AC-MnO_x attracted NH_4^+ into its surface. In addition, NH_4^+ ions entered the cation tunnel of MnO_x through electrostatic adsorption and occupied oxygen vacancies (Wang and Li 2003). With the high oxidation activity of Mn(III), the reaction between Mn(III) and NH_4^+ ions led to form Mn(II) and nitrate (Eq. (12)). The electrostatic repulsion between AC-MnO_x and the negative charged ions (such as chloride ions, nitrate, and nitrite) decreased, thereby reducing their influence on the adsorption process and promoting the release of them into the solution. After finishing the catalytic oxidation, AC-MnO_x continued to adsorb ammonium.

CW application of AC-MnO_x on ammonium removal

The CW construction and operating parameters are shown in the Fig. S13 and Table S8, respectively. Figure 8 shows the impact of AC-MnO_x on ammonium removal performance in CWs. After 1 day of feeding CWs with NH_4^+-N synthesis wastewater, the average NH_4^+-N removal efficiency in the AC-MnO_x filling regions reached 69.37%, while it was 23.87% in the AC region, and only 7.08% in the inert CW-control (Fig. 8a). The average NH_4^+-N removal rates for these three groups were 28.04, 13.08, and 3.88 mg/(m^3·h), respectively. As the HRT increased from 1 to 3 days, the NH_4^+-N removal efficiency improved, but the removal rate decreased due to the slower adsorption rate of the adsorbent. The highest removal rate achieved in the AC-MnO_x filling regions was 92.6%. To investigate the response of AC-MnO_x fillers to high nitrogen loads, the influent NH_4^+-N concentration was increased to 15 mg/L after 5 cycles of operation (Fig. 8b). The results showed that the average NH_4^+-N removal rate significantly increased for all three CWs, with the highest 64.97 mg/(m^3·h) in CW-AC-MnO_x at an HRT of 1 day. This illustrated that AC-MnO_x provided a favorable environment for microorganisms. Whereafter, the CWs were operated in continuous flow mode, and the removal rate of CW-AC-MnO_x reached a high 112.89 mg/(m^3·h) (Fig. 8c). Overall, the use of AC-MnO_x significantly improved the nitrogen removal performance of CW and demonstrated its ability to synergistically remove nitrogen with the action of microorganisms.

Conclusion

In this study, MnO_x was loaded on the surface of AC for ammonium removal. Ammonium removal experiments showed that the ammonium removal performance of the synthesized material was improved after loading on the MnO_x film (15.6 times than before). The dosage is the main factor affecting the removal of ammonium. The ammonium removal process by AC-MnO_x involved adsorption and catalytic conversion, and the latter reacted more slowly than the former. Besides, the increase in initial concentration improved the proportion of adsorption. The ammonium removal mechanism by AC-MnO_x included ion exchange, electrostatic adsorption, and catalytic oxidation. Overall, this work proposed a novel strategy for engineering practices in nutrient removal and provided theoretical support for a profound understanding of the remediation process. Future research efforts should focus on the long-term performance of AC-MnO_x in continuous removal of ammonium wastewater.

Supplementary Information The online version contains supplementary material available at https://doi.org/10.1007/s11356-023-30086-7.

Author contribution Yifei Wang: writing—original draft and writing—review and editing; Xinyi Jiang: experimental design, and writing—original draft; Xinshan Song: writing—review and editing, supervision, and funding acquisition; Xin Cao: funding acquisition, data curation, and formal analysis; Zhongshuo Xu, Yuhui Wang, Jianfeng Li, Nan Wu, and Junhong Bai: conceptualization, validation, methodology, investigation, project administration, and supervision.

Funding This work was supported by the National Natural Science Foundation of China (Grant No. 52170152), the Science and Technology Innovation Action Plan Social Development Key Science and Technology Project of Shanghai (No. 21DZ1202402), the National key research and development project (No. 2021YFC3000102), the Youth Program of National Natural Science Foundation of China (Grant No. 51909034), and the Fundamental Research Funds for the Central Universities and Graduate Student Innovation Fund of Donghua University (No. CUSF-DH-D-2022066).

Data availability The authors declare that the main data supporting the findings of this study are contained within the paper and its associated supplementary information. All other relevant data are available from the corresponding author upon reasonable request.

Declarations

Ethical approval Not applicable.

Consent to participate The work described is original work of authors.

Consent to publish The work has not been submitted elsewhere for publication. The authors have provided consent to publish this work.

Competing interests The authors declare no competing interests.

References

Andersson A, Laurent P, Kihn A (2001) Impact of temperature on nitrification in biological activated carbon (BAC) filters used for drinking watertreatment. Water Res 35(12):2923–2934. https://doi.org/10.1016/S0043-1354(00)00579-0

Benhiti R, Ait Ichou A, Zaghloul A, Aziam R, Carja G, Zerbet M, Sinan F, Chiban M (2020) Synthesis, characterization, and comparative study of MgAl-LDHs prepared by standard coprecipitation and urea hydrolysis methods for phosphate removal. Environ Sci Pollut Res 27(36):45767–45774. https://doi.org/10.1007/s11356-020-10444-5

Bhatnagar A, Hogland W, Marques M, Sillanpää M (2013) An overview of the modification methods of activated carbon for its water

treatment applications. Chem Eng J 219:499–511. https://doi.org/10.1016/j.cej.2012.12.038
Cai YA, Li D, Liang Y, Luo Y, Zeng H, Zhang J (2015) Effective start-up bio-filtration method for Fe, Mn, and ammonia removal and bacterial community analysis. Bioresour Technol 176:149–155. https://doi.org/10.1016/j.biortech.2014.11.025
Cai Z, Deng X, Wang Q, Lai J, Xie H, Chen Y, Huang B, Lin G (2020) Core-shell granular activated carbon and its adsorption of trypan blue. J Clean Prod 242. https://doi.org/10.1016/j.jclepro.2019.118496
Chen M, Wu J, Qiu X, Jiang L, Wu P (2023) The important role of the interaction between manganese minerals and metals in environmental remediation: a review. Environ Sci Pollut Res Int 30:39319–39337. https://doi.org/10.1007/s11356-023-25575-8
Cheng S, Zhang L, Xia H, Peng J, Shu J, Li C, Jiang X, Zhang Q (2017a) Adsorption behavior of methylene blue onto waste-derived adsorbent and exhaust gases recycling. RSC Adv 7(273):31–41. https://doi.org/10.1039/c7ra01482a
Cheng Y, Huang T, Sun Y, Shi X (2017b) Catalytic oxidation removal of ammonium from groundwater by manganese oxides filter: performance and mechanisms. Chem Eng J 322:82–89. https://doi.org/10.1016/j.cej.2017.04.010
Cheng Y, Huang T, Cheng L, Sun Y, Zhu L, Li Y (2018) Structural characteristic and ammonium and manganese catalytic activity of two types of filter media in groundwater treatment. J Environ Sci (china) 72:89–97. https://doi.org/10.1016/j.jes.2017.12.014
Cheng H, Zhu Q, Xing Z (2019) Adsorption of ammonium in low temperature domestic wastewater by modification bentonite. J Clean Prod 233. https://doi.org/10.1016/j.jclepro.2019.06.079
Chiban M, Soudani A, Sinan F, Persin M (2011a) Single, binary and multi-component adsorption of some anions and heavy metals on environmentally friendly Carpobrotus edulis plant. Colloids Surf B 82(2):267–276. https://doi.org/10.1016/j.colsurfb.2010.09.013
Chiban M, Soudani A, Sinan F, Tahrouch S, Persin M (2011b) Characterization and application of dried plants to remove heavy metals, nitrate, and phosphate ions from industrial wastewaters. CLEAN - Soil, Air, Water 39(4):376–383. https://doi.org/10.1002/clen.201000127
Ducey TF, Vanotti MB, Shriner AD, Szogi AA, Ellison AQ (2010) Characterization of a microbial community capable of nitrification at cold temperature. Bioresour Technol 101(2):491–500. https://doi.org/10.1016/j.biortech.2009.07.091
Egbosiuba TC, Abdulkareem AS, Kovo AS, Afolabi EA, Tijani JO, Auta M, Roos WD (2020) Ultrasonic enhanced adsorption of methylene blue onto the optimized surface area of activated carbon: adsorption isotherm, kinetics and thermodynamics. Chem Eng Res Des 153. https://doi.org/10.1016/j.cherd.2019.10.016
Forrez I, Carballa M, Noppe H, Brabander H, Boon N, Verstraete W (2009) Influence of manganese and ammonium oxidation on the removal of 17α-ethinylestradiol (EE2). Water Res 43(1):77–86. https://doi.org/10.1016/j.watres.2008.10.006
Gadde RR, Laitinen HA (1974) Heavy metal adsorption by hydrous iron and manganese oxides. Anal Chem 46(13):2022–2026. https://doi.org/10.1021/ac60349a004
Girotto P, Sílvia D, Élvio A (2020) Chrysotile asbestos treated with phosphoric acid as an adsorbent for ammonium. Heliyon 6(2). https://doi.org/10.1016/j.heliyon.2020.e03397
Guo Y, Huang T, Wen G, Cao X (2017) The simultaneous removal of ammonium and manganese from groundwater by iron-manganese co-oxide filter film: the role of chemical catalytic oxidation for ammonium removal. Chem Eng J 308:322–329. https://doi.org/10.1016/j.cej.2016.09.073
Hu B, Ai Y, Jin J, Hayat T, Alsaedi A, Zhuang L, Wang X (2020) Efficient elimination of organic and inorganic pollutants by biochar and biochar-based materials. Biochar 2:47–64. https://doi.org/10.1007/s42773-020-00044-4
Huang TL, Cao X, Zhang Q, Su ZM, Zheng N (2014) Catalytic oxidation of high-concentration ammonia in groundwater by a naturally formed co-oxide filter film. Desalin Water Treat 52(7–9):1615–1623. https://doi.org/10.1080/19443994.2013.848652
Joshi T, Zhang G, Cheng H, Liu R, Liu H, Qu J (2017) Transformation of para arsanilic acid by manganese oxide: adsorption, oxidation, and influencing factors. Water Res 126–134. https://doi.org/10.1016/j.watres.2017.03.028
Kankanamge J, Chour NR, Welsh C, Li DT, Teasdale T (2018) Removing ammonium from water and wastewater using cost-effective adsorbents: a review. J Inst Environ Sci 63:174–197. https://doi.org/10.1016/j.jes.2017.09.009
Karthikeyan M, Satheeshkumar KK, Elango KP (2008) Removal of fluoride ions from aqueous solution by conducting polypyrrole. J Hazard Mater 167(1):300–305. https://doi.org/10.1016/j.jhazmat.2008.12.141
Kim SC, Shim WG (2010) Catalytic combustion of VOCs over a series of manganese oxide catalysts. Appl Catal B Environ 98(3–4):180–185. https://doi.org/10.1016/j.apcatb.2010.05.027
Kizito S, Wu S, Kipkemoi K, Lei W, Lu M, Bah H, Dong R (2015) Evaluation of slow pyrolyzed wood and rice husks biochar for adsorption of ammonium nitrogen from piggery manure anaerobic digestate slurry. Sci Total Environ 505:102–112. https://doi.org/10.1016/j.scitotenv.2014.09.096
Kołodziej A, Fuentes M, Baigorri R, Lorenc GE, García MJM, Burg P, Gryglewicz G (2014) Mechanism of adsorption of different humic acid fractions on mesoporous activated carbons with basic surface characteristics. Adsorption 20(2014):667–675. https://doi.org/10.1007/s10450-014-9610-3
Kumar A, Sanger A, Kumar A, Kumar Y, Chandra R (2016) An efficient α-MnO_2 nanorods forests electrode for electrochemical capacitors with neutral aqueous electrolytes. Electrochim Acta 220. https://doi.org/10.1016/j.electacta.2016.10.168
Lee SM, Lalhmunsiama, Choi SI, Tiwari D (2013) Manganese and iron oxide immobilized activated carbons precursor to dead biomasses in the remediation of cadmium-contaminated waters. Environ Sci Pollut Res Int 20(10):7464–77. https://doi.org/10.1007/s11356-013-1609-x
Lee W, Yoon S, Choe JK, Lee M, Choi Y (2018) Anionic surfactant modification of activated carbon for enhancing adsorption of ammonium ion from aqueous solution. Sci Total Environ 639:1432–1439. https://doi.org/10.1016/j.scitotenv.2018.05.250
Li X, Chu Z, Liu Y, Zhu M, Yang L, Zhang J (2013) Molecular characterization of microbial populations in full-scale biofilters treating iron, manganese and ammonia containing groundwater in Harbin, China. Bioresour Technol 147:234–239. https://doi.org/10.1016/j.biortech.2013.08.008
Li W, Cui X, Zeng R, Du G, Sun Z, Zheng R, Ringer SP, Dou SX (2015a) Performance modulation of α-MnO_2 nanowires by crystal facet engineering. Sci Rep 5:8987. https://doi.org/10.1038/srep08987
Li X, Blatchley W, Wang X, Ren P (2015b) UV-chlorine process for ammonia removal and disinfection by-product reduction: comparison with chlorination. Water Res 68:804–811. https://doi.org/10.1016/j.watres.2014.10.044
Li R, Wang JJ, Zhou B, Zhang Z, Liu S, Lei S, Xiao R (2017) Simultaneous capture removal of phosphate, ammonium and organic substances by MgO impregnated biochar and its potential use in swine wastewater treatment. J Clean Prod 147:96–107. https://doi.org/10.1016/j.jclepro.2017.01.069
Li Z, Hanafy H, Zhang L, Sellaoui L, Schadeck Netto M, Oliveira MLS, Seliem MK, Luiz Dotto G, Bonilla-Petriciolet A, Li Q (2020) Adsorption of Congo red and methylene blue dyes on an Ashitaba waste and a walnut shell-based activated carbon from aqueous solutions: experiments, characterization and physical

interpretations. Chem Eng J 388:124263. https://doi.org/10.1016/j.cej.2020.124263
Li Y, Bai X, Ding R, Lv W, Long Y, Wei L, Xiang F, Wang R (2021) Removal of phosphorus and ammonium from municipal wastewater treatment plant effluent by manganese ore in a simulated constructed wetland. Environ Sci Pollut Res Int 28:41169–41180. https://doi.org/10.1007/s11356-021-13555-9
Lin H, Taillefert M (2014) Key geochemical factors regulating Mn(IV)-catalyzed anaerobic nitrification in coastal marine sediments. Geochim Cosmochim Acta 133:17–33. https://doi.org/10.1016/j.gca.2014.01.025
Liu Y, Ngo HH, Guo W, Peng L, Wang D, Ni B (2019) The roles of free ammonia (FA) in biological wastewater treatment processes: a review. Environ Int 123:10–19. https://doi.org/10.1016/j.envint.2018.11.039
Liu D, Tian J, Tang Y, Li J, Wu S, Yi S, Huang X, Sun D, Wang H (2021) High-power double-face flow Al-air battery enabled by CeO_2 decorated MnOOH nanorods catalyst. Chem Eng J 406(15). https://doi.org/10.1016/j.cej.2020.126772
Lyu Y, Liu X, Liu W, Tian Y, Qin Z (2020) Adsorption/oxidation of ethyl mercaptan on Fe-N-modified active carbon catalyst. Chem Eng J 393(1). https://doi.org/10.1016/j.cej.2020.124680
Meng Y, Zhao K, Zhang Z, Gao P, Yuan J, Cai T, Tong Q, Huang G, He D (2020) Effects of crystal structure on the activity of MnO_2 nanorods oxidase mimics. Nano Res 13(3):709–718. https://doi.org/10.1007/s12274-020-2680-5
Nguyen V-T, Vo T-D-H, Tran T, Nguyen T-N, Le T-N-C, Bui X-T, Bach L-G (2021) Biochar derived from the spent coffee ground for ammonium adsorption from aqueous solution. Case Stud Chem Environ Eng 4:100141. https://doi.org/10.1016/j.cscee.2021.100141
Nouaa S, Aziam R, Benhiti R, Carja G, Iaich S, Zerbet M, Chiban M (2023) Synthesis of LDH/alginate composite beads as a potential adsorbent for phosphate removal: kinetic and equilibrium studies. Chem Pap. https://doi.org/10.1007/s11696-023-02969-z
Peng X, Wang M, Hu F, Qiu F, Zhang T, Dai H, Cao Z (2018) Multipath fabrication of hierarchical CuAl layered double hydroxide/carbon fiber composites for the degradation of ammonium. Environ Manag 220:173–182. https://doi.org/10.1016/j.jenvman.2018.05.037
Qiang J, Zhou Z, Wang K, Qiu Z, Zhi H, Yuan Y, Zhang Y, Jiang Y, Zhao X, Wang Z, Wang Q (2020) Coupling ammonium adsorption and regeneration unit with a high-load anoxic/aerobic process to achieve rapid and efficient pollutants removal for wastewater treatment. Water Res 170. https://doi.org/10.1016/j.watres.2019.115280
Rajeshwari KV, Balakrishnan M, Kansal A, Lata K, Kishore V (2000) State-of-the-art of anaerobic digestion technology for industrial wastewater treatment. Renew Sustain Energy Rev 4(2):135–156. https://doi.org/10.1016/S1364-0321(99)00014-3
Schüler C, Betzenbichler F, Drescher C, Hinrichsen O (2018) Optimization of the synthesis of Ni catalysts via chemical vapor deposition by response surface methodology. Chem Eng Res Des 132:303–312. https://doi.org/10.1016/j.cherd.2018.01.015
Shafiof MS, Ejhieh AN (2020) A comprehensive study on the removal of Cd (II) from aqueous solution on a novel pentetic acid-clinoptilolite nanoparticles adsorbent: experimental design, kinetic and thermodynamic aspects. Solid State Sci 99. https://doi.org/10.1016/j.solidstatesciences.2019.106071
Sharma RK, Zhai L (2009) Multiwall carbon nanotube supported poly (3,4-ethylenedioxythiophene)/manganese oxide nanocomposite electrode for super-capacitors. Electrochim Acta 54:7148–7155. https://doi.org/10.1016/j.electacta.2009.07.048
Sheela T, Nayaka YA, Viswanatha R, Basavanna S, Venkatesha TG (2012) Kinetics and thermodynamics studies on the adsorption of Zn (II), Cd (II) and Hg (II) from aqueous solution using zinc oxide nanoparticles. Powder Technol 217:163–170. https://doi.org/10.1016/j.powtec.2011.10.023
Shen Q, Wang Z, Yu Q, Cheng Y, Liu Z, Zhang T, Zhou S (2020) Removal of tetracycline from an aqueous solution using manganese dioxide modified biochar derived from Chinese herbal medicine residues. Environ Res 183:109195. https://doi.org/10.1016/j.envres.2020.109195
Shi M, Wang Z, Zheng Z (2013) Effect of Na^+ impregnated activated carbon on the adsorption of NH^+_4-N from aqueous solution. J Environ Sci 25:1501–1510. https://doi.org/10.1016/S1001-0742(8)60227-7
Subramanian S, Zhu H, Wei B (2006) Nanostructured MnO_2: Hydrothermal synthesis and electrochemical properties as a supercapacitor electrode material. J Power Sources 159(1):361–364. https://doi.org/10.1016/j.jpowsour.2006.04.012
Takaya CA, Fletcher LA, Singh S, Anyikude KU, Ross AB (2016) Phosphate and ammonium sorption capacity of biochar and hydrochar from different wastes. Chemosphere 145:518–527. https://doi.org/10.1016/j.chemosphere.2015.11.052
Tan M, Li Y, Chi D, Wu Q (2023) Efficient removal of ammonium in aqueous solution by ultrasonic magnesium-modified biochar. Chem Eng J 461:142072. https://doi.org/10.1016/j.cej.2023.142072
Tatari K, Smets BF, Albrechtsen J (2016) Depth investigation of rapid sand filters for drinking water production reveals strong stratification in nitrification biokinetic behavior. Water Res 101:402–410. https://doi.org/10.1016/j.watres.2016.04.073
Tebo BM, Johnson HA, McCarthy JK, Templeton AS (2005) Geomicrobiology of manganese (II) oxidation. Trends Microbiol 13(9):421−428. https://doi.org/10.1016/j.tim.2005.07.009
Toupin N, Brousse T, Bélanger D (2004) Charge storage mechanism of MnO_2 electrode used in aqueous electrochemical capacitor. Chem Mater 16:3148. https://doi.org/10.1021/cm049649
Uğurlu M, Karaoğlu MH (2011) Adsorption of ammonium from an aqueous solution by fly ash and sepiolite: isotherm, kinetic and thermodynamic analysis. Microporous Mesoporous Mater 139:173–178. https://doi.org/10.1016/j.micromeso.2010.10.039
Vocciante M, D'Auris A, Finocchi A, Tagliabue M, Bellettato M, Ferrucci A, Reverberi A, Ferro S (2018) Adsorption of ammonium on clinoptilolite in presence of competing cations: investigation on groundwater remediation. J Clean Prod 198:480–487. https://doi.org/10.1016/j.jclepro.2018.07.025
Wang X, Li Y (2003) Synthesis and formation mechanism of manganese dioxide nanowires/nanorods. Chemistry 9(1):300–306. https://doi.org/10.1002/chem.200390024
Wang Q, Yang P, Zhu M (2018) Structural transformation of birnessite by fulvic acid under anoxic conditions. Environ Sci Techonol 52(4):1844–1853. https://doi.org/10.1021/acs.est.7b04379
Wang Y, Song X, Cao X, Xu Z, Huang W, Wang Y et al (2022) Integration of manganese ores with activated carbon granules into CW-MFC to trigger anoxic electron transfer and removal of ammonia nitrogen. J Clean Prod 334:130202. https://doi.org/10.1016/j.jclepro.2021.130202
Wang H, Chen Q, Liu R, Xia H, Zhang Y (2023) Enhanced removal performance and mechanism of NH_4^+/NO_3^- in starch-FeS-biochar-amended vertical flow constructed wetlands under Pb stress. J Water Process Eng 55:104170. https://doi.org/10.1016/j.jwpe.2023.104170
Wang M, Zhang P, Li J, Jiang C (2014) The effects of Mn loading on the structure and ozone decomposition activity of MnO_x supported on activated carbon. Chin J Catal 35(3). https://doi.org/10.1016/S1872-2067(12)60756-6
Xie H, Yang Y, Liu J, Kang Y, Zhang J, Hu Z, Liang S (2018) Enhanced triclosan and nutrient removal performance in vertical up-flow constructed wetlands with manganese oxides. Water Res 143:457–466. https://doi.org/10.1016/j.watres.2018.05.061

Xue H, Gao X, Seliem MK, Mobarak M, Dong R, Wang X, Fu K, Li Q, Li Z (2023) Efficient adsorption of anionic azo dyes on porous heterostructured MXene/biomass activated carbon composites: experiments, characterization, and theoretical analysis via advanced statistical physics models. Chem Eng J 451:138735. https://doi.org/10.1016/j.cej.2022.138735

Yang H, Li D, Zeng H, Zhang J (2019) Long-term operation and autotrophic nitrogen conversion process analysis in a biofilter that simultaneously removes Fe, Mn and ammonia from low-temperature groundwater. Chemosphere 222. https://doi.org/10.1016/j.chemosphere.2019.01.143

Zhang N, Yang Y, Huang L, Xie H, Hu Z (2019) Birnessite-coated sand filled vertical flow constructed wetlands improved nutrients removal in a cold climate. RSC Adv 9(62):35931–35938. https://doi.org/10.1039/c9ra07364g

Zhang L, Wang J, Qiao H, Liu F, Fu Z (2020) Synthesis of manganese oxides for adsorptive removal of ammonia nitrogen from aqueous solutions. J Clean Prod 272:123055. https://doi.org/10.1016/j.jclepro.2020.123055

Zhao S, Yi H, Tang X, Gao F, Zhang B, Wang Z, Zuo Y (2015) Methyl mercaptan removal from gas streams using metal-modified activated carbon. J Clean Prod 87:856–861. https://doi.org/10.1016/j.jclepro.201.10.001

Zhao S, Wang Q, Sun J, Borkiewicz OJ, Huang R, Saad EM, Fields B, Chen S, Zhu M, Tang Y (2018) Effect of Zn coprecipitation on the structure of layered Mn oxides. Chem Geol 493:234–245. https://doi.org/10.1016/j.chemgeo.2018.05.044